# Multiterminal transport measurements: In-plane anisotropy and vortex liquid correlation in $YBa_2Cu_3O_{7-\delta}$

T. Björnängen,* A. Rydh, and Ö. Rapp
*Solid State Physics, Royal Institute of Technology, SE-100 44 Stockholm, Sweden*
(Received 9 July 2001; published 20 November 2001)

Using a modified pseudoflux transformer geometry, the in-plane anisotropy and vortex-liquid correlation of an untwinned $YBa_2Cu_3O_{7-\delta}$ single crystal have been studied. The square-shaped, multiterminal sample design allows comparative studies of *a*- and *b*-axis properties for arbitrarily oriented magnetic fields. We compare the in-plane resistivity in the case of intrinsic pinning with the longitudinal resistivity, i.e., with the resistivity in absence of a macroscopic Lorentz force. The relative ratio between resistivities $\rho_a$ and $\rho_b$ in the vortex state can be made to vary over a wide range by controlling the direction of the applied magnetic field. Evidence is found for almost isotropic fluctuations corresponding to a fluctuation anisotropy $\gamma_{ab}^{\mathrm{fl}} \approx 1.1$, noted to be clearly lower than the anisotropy $\gamma_{ab} = 1.27$ obtained from the vortex phase diagram.

DOI: 10.1103/PhysRevB.64.224510 PACS number(s): 74.25.Fy, 74.60.Ge

## I. INTRODUCTION

There are several open questions concerning the field-temperature ($H-T$) phase diagram of the high-$T_c$ superconductors. One of the major challenges is the nature of the vortex liquid. Early studies through multiterminal measurements with the magnetic field parallel to the crystallographic *c* axis suggested that the vortex liquid in $Bi_2Sr_2CaCu_2O_{8+\delta}$ (Bi-2212) is uncorrelated in all directions,[1,2] while the correlation along the vortex lines in twinned $YBa_2Cu_3O_{7-\delta}$ (YBCO) is lost within the liquid phase.[3–5] Clean, untwinned YBCO undergoes a first-order, solid-to-liquid transition at a melting temperature $T_m$,[6,7] and was first reported by López *et al.* to display an uncorrelated liquid.[8]

It has now been well established, both from numerical simulations,[9–11] and from multiterminal measurements[8] that global phase coherence is lost when entering the vortex-liquid state. The liquid is thus dissipative in all directions, including the longitudinal one along the magnetic field. It is important to note, however, that the loss of superconducting coherence does not imply a system of decoupled pancakes above $T_m$. The liquid still consists of vortex lines[12–15] with finite (long wavelength) line tension at least close to $T_m$.[16,17] The system is instead denoted *entangled* since the longitudinal vortex correlation is lost in the limit of infinitely thick samples. The degree and structure of the entanglement is an open question. It is clear, though, from the large Lorentz force contribution to the resistivity in clean samples,[15,18] that the entanglement is on a scale much longer than the interplanar distance. The vortices will, in other words, be relatively straight as long as the direction of the applied magnetic field has a significant influence on vortex motion and dissipation, even though a longitudinal current cannot be maintained without dissipation.

From resistive measurements on untwinned YBCO, Righi *et al.* found the velocity correlation length to be a few micrometers just above $T_m$,[12] and multiterminal measurements by Rydh and Rapp[15] indicated even stronger longitudinal correlation in the liquid. Theoretical simulations seem to give much shorter correlation lengths,[19] but are hard to compare with experiments since a direct connection between correlation length and resistivity is lacking. The mechanism behind the nonzero vortex-liquid resistivity in absence of a net Lorentz force is thus clearly connected to the question of vortex correlation. From a technological point of view it would be valuable to control this dissipation or at least to be able to predict its magnitude. The excess resistivity, i.e., the difference in $\rho$ between $\mathbf{H} \perp \mathbf{j}$ and $\mathbf{H} \parallel \mathbf{j}$, is much easier to take into account since it can be described as a Lorentz-force-driven flux motion.[18]

In this paper, we present new, symmetric, pseudoflux transformer (PFT) measurements on untwinned YBCO, allowing comparisons of in-plane resistivities for different field directions on the same crystal. We compare resistivities parallel and perpendicular to the field and calculate the Lorentz force contribution. The latter seems to have its maximum within the vortex liquid and extend up to just around $T_c$. For **H** perfectly aligned within the *ab* plane, intrinsic pinning suppresses the melting steps of the transversal resistivity $\rho_\perp$, but is argued not to destroy the first-order character of the transition. In- and out-of-plane anisotropies are determined from the $H-T$ phase diagram of the melting transition. The observed rapid change of the *ab*-plane anisotropy with temperature around $T_c$ is explained as an effect of almost isotropic superconducting fluctuations.

## II. EXPERIMENTAL

YBCO single crystals were grown using a standard self-flux method,[20] and annealed in $O_2$ at 400 °C for 6 days. A plate-shaped crystal with approximate size $330 \times 350 \times 10\ \mu m^3$ and zero resistance $T_c$ just above 92 K was chosen and verified in a polarized light microscope to be untwinned. Epoxy silver paint (EPO-TEK H20E) was used to apply eight contacts, two on each side, as shown in the inset of Fig. 1. All measurements were made with a current $I = 50\ \mu A$, lying well within the Ohmic response regime of the vortex liquid. A dc picovoltmeter with a voltage resolution around 0.3 nV was used as a preamplifier throughout the measurements. Voltages were measured during slow temperature sweeps while scanning the current. Magnetic fields

 

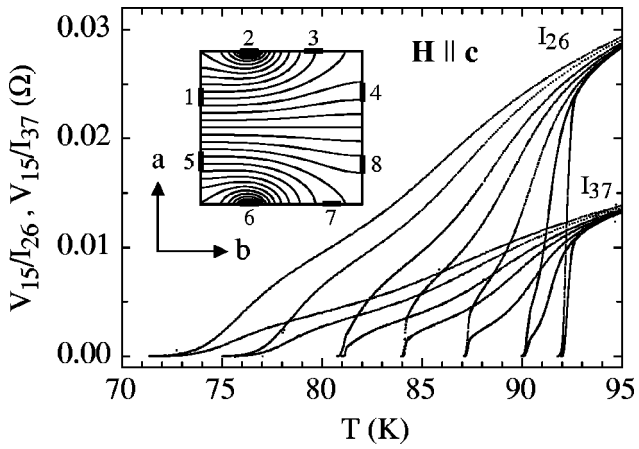


FIG. 1. Measured voltage $V_{15}$ as a function of current path ($I_{26}$ and $I_{37}$, $I=50\ \mu$A), temperature, and magnetic field. The fields are given by $\mu_0 H = 12$, 9, 6, 4, 2, 0.5, and 0 T (from left to right). Inset: Equipotential curves for current $I_{26}$ (i.e., current flowing between contacts 2 and 6) at an anisotropy value $\gamma_{ab}=1.36$ reflecting the typical normal-state distribution or the **H** ∥ **c** case. Actual contact positions are shown.

up to 12 T were applied both in plane and out of plane, as well as slightly off the $ab$ plane and within the $bc$ plane, using a rotatable sample holder with an angular resolution of 0.01°.

## III. RESULTS AND DISCUSSION

### A. Effects of the magnetic field direction

In Fig. 1 experimental data for fields parallel to the $c$ axis are shown. Unlike the conventional PFT configuration, this setup probes intervortex correlations when **H** ∥ **c**. No current is flowing along the field direction, and, therefore, the *longitudinal* vortex-line correlation strength does not influence the studied voltages. We find that the system is well described by local conductivity, so that the ratio between $V_{15}(I_{37})$ and $V_{15}(I_{26})$ is determined exclusively by sample/contact geometry and anisotropic properties. Intervortex correlations are consequently weak, i.e., the vortex-liquid viscosity is low enough to have negligible effect on the vortex flow on the scale of the sample. Melting steps can be clearly seen for fields from 0.5 to 6 T but there is no step at 9 or 12 T. Comparing the response at low and high fields, the voltage ratio reveals no qualitative change when crossing the upper critical point, located between 6 and 9 T.

The inset of Fig. 1 also shows equipotential curves obtained by using a finite difference method to solve the Laplace equation, assuming local conductivity. The Laplace equation can be expressed with resistivity and in-plane anisotropy $\gamma_{ab}$ as independent parameters. The anisotropy is, therefore, directly related to, for instance, the ratio $V_{15}(I_{37})/V_{15}(I_{26})$. Various voltage ratios are in practice precalculated as a function of anisotropy and later used to determine the actual anisotropy from measurements. The assumption of local conductivity can be checked by comparing $\gamma_{ab}$ for different current distributions, and has previously been used to successfully model, for instance, the vortex liquid of YBCO in the Corbino disc geometry.[21]

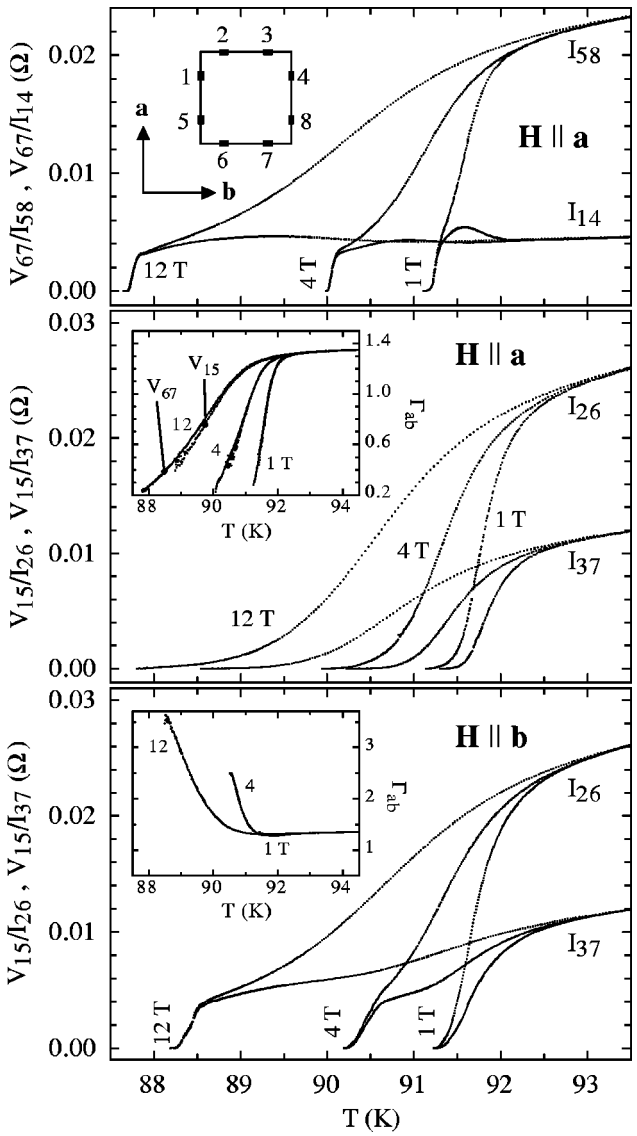


FIG. 2. Top: Resistive transition in the Lorentz-force configuration with the magnetic field aligned 1° away from the $a$ axis. Close to $T_m$ the difference in $V/I$ for the two current paths vanishes, indicating that $\rho_a$ is small. Middle: With the current flowing mainly along the magnetic field, the macroscopic Lorentz force gives no net contribution to $V_{15}$. The inset shows a comparison of the in-plane resistive ratio $\Gamma_{ab}$ as calculated from measurements of $V_{67}(I_{14},I_{58})$ (top panel) and $V_{15}(I_{26},I_{37})$ (middle panel), respectively, with **H** directed 1° from the $a$ axis. Bottom: With the same current contacts as in the middle panel, but with **H** aligned 1° away from the $b$ axis, the Lorentz contribution is recovered. Also note the increased $\Gamma_{ab}$ in the vortex state (inset), the shift in $T_m$ when comparing with the top panel, and the disappearance of the melting step at around 1 T.

In the measurements presented in Fig. 2, we applied the field almost parallel to the $ab$ plane. It was not aligned exactly within the plane, since intrinsic pinning would have set in and suppressed the vortex flow and possible melting steps. The range of intrinsic pinning can be estimated from the dip

observed in the angular dependence of $\rho(\vartheta)$ around $\vartheta = 0°$ (**H** ∥ **ab**). The width of the dip is typically found to be of the order of 0.5°.[22] To be able to detect changes in the Lorentz force contribution, we, therefore, chose to apply the field 1° away from the *ab* plane. This is outside the dip, having a total width ~0.7° in our sample, but close enough to the *ab* plane not to significantly alter the magnitude of the Lorentz force.

In the top panel of Fig. 2 the field was aligned almost parallel to the *a* axis while the current was sent mainly along the *b* axis, so that the field was mainly perpendicular to the current. In this case there is, thus, a net Lorentz force directed along the *c* axis. Clear melting steps can be seen for all fields. The *V*/*I* curves of the two current paths coincide close to the melting transition, indicating that $\rho_a$ is small. This is supported by the results in the middle panel, where the current is sent along the *a* axis, i.e., with the field mainly parallel to the current. The different current path curves then differ even around $T_m$, as they would if $\rho_b$ is large compared to $\rho_a$. Without a net macroscopic Lorentz force the melting steps disappear completely, leaving smoothly vanishing tails. This suggests that the step feature is caused solely by Lorentz-force-induced dissipation. Note that the vortex configuration remains unchanged between the top and middle panels. In the vortex solid the pinned lattice is immobile at low currents, but the amount of defects is too low for all vortices to become individually pinned in the not-so-viscous liquid. Hence the Lorentz force suddenly becomes free to act when crossing $T_m$.

We find good agreement between the in-plane resistive ratios $\Gamma_{ab} = (\rho_a/\rho_b)^{1/2}$ calculated from different current paths (see inset, middle panel of Fig. 2). If the conductivity would display nonlocal behavior, one could instead expect clear discrepancies. A local conductivity picture combined with Lorentz-force arguments is, thus, used to explain also the results of Fig. 2.

To further study the Lorentz-force configuration, we applied the field (almost) along the *b* axis, while keeping the main current direction from the middle panel, so that the current again is perpendicular to the field. As seen in the bottom panel, the typical signs of the melting transition are recovered. Following the Lorentz-force picture, the coincidence of the *V*/*I* curves close to $T_m$ suggests that, for this field direction, $\rho_b$ is small close to $T_m$. The additional Lorentz-force resistivity has, thus, been added to $\rho_a$ instead. The top and bottom panels show quite similar behavior, but some differences can be noted. First, the effect of in-plane anisotropy is reflected by a shift in $T_m$, increasing with increasing magnetic field. Second, the melting step at 1 T has almost disappeared, indicating a possible field-directional dependence of the lower critical point.

In the inset of the bottom panel of Fig. 2, we show $\Gamma_{ab}$ for the **H** ∥ **b** case. Comparing with the middle panel inset, it is seen that the ratio decreases rapidly with decreasing temperature for **H** ∥ **a**, while the opposite is true when the field is directed along the *b* axis. $\Gamma_{ab}$ may thus depend both on field direction and strength, but should not vary with current distribution if local conductivity is to hold. It is clear that $\Gamma_{ab}$ cannot represent the in-plane anisotropy $\gamma_{ab}$ in the vortex liquid, and we therefore use separate notations.

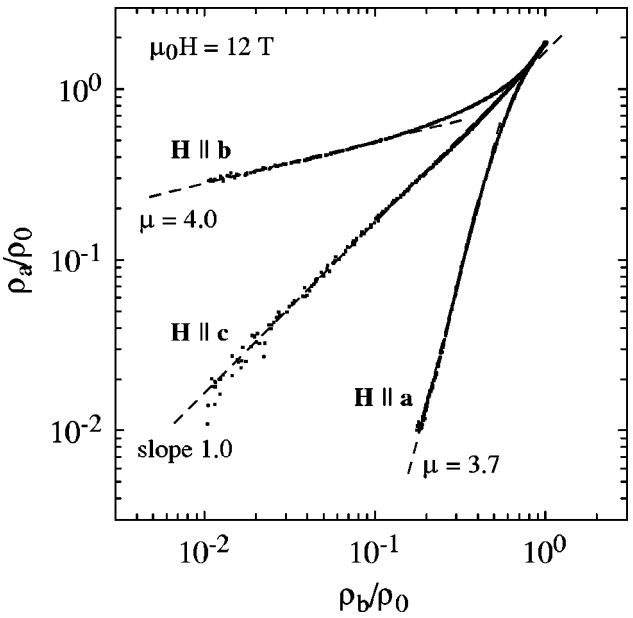


FIG. 3. Resistivity along the *a* axis as a function of the *b*-axis resistivity at 12 T for the three main field directions. (For **H** ∥ **a** and **H** ∥ **b** the field is aligned 1° away from the plane to avoid the intrinsic pinning.) The constant $\rho_0$ is arbitrarily defined as $\rho_b$ at 96 K. The exponent $\mu$ is defined through the relation $\rho_\parallel \sim \rho_\perp^\mu$.

At least two scenarios have been suggested for the gradual change from a vortex system with a preferential direction to the state without any signs of the Lorentz force; either the vortices entangle or they decouple into pancake vortices in the $CuO_2$ layers. If the coupling strength between neighboring pancake vortices would be a critical parameter for the vortex-liquid behavior one could expect the correlation strength to be sensitive to the orientation of the magnetic field relative to the layered structure. Such a dependence is not seen. The transitions with **H** within the *ab* plane closely resemble the case with **H** ∥ **c** (e.g., Refs. 8, 21, or 23). We therefore believe that this kind of decoupling is not dominant in YBCO. Since the present measurements and our earlier results[15] are in strong favor of the local-conductivity model, we further argue that the vortex-liquid behavior is independent of the sample dimensions (as long as the sample is three dimensional). This means that there is no shortest length scale over which vortices entangle and below which dissipation would be zero due to relatively straight, disentangled vortices. With an entangled state we, thus, mean any state allowing a simple line bending.

To obtain a quantitative measure of the dissipation in the vortex liquid, we further investigated the relation between $\rho_a$ and $\rho_b$ for the three main magnetic-field directions, as shown in Fig. 3. It is seen that there is a connection between longitudinal and transversal resistivity, which can be described by the expression $\rho_\parallel \sim \rho_\perp^\mu$. For **H** ∥ **a** we find an exponent $\mu = 3.7$, while for **H** ∥ **b** we obtain $\mu = 4.0$. The case with **H** ∥ **c** is just a comparison of two $\rho_\perp$ resistivities and thus yields a slope 1.0 to a good approximation.

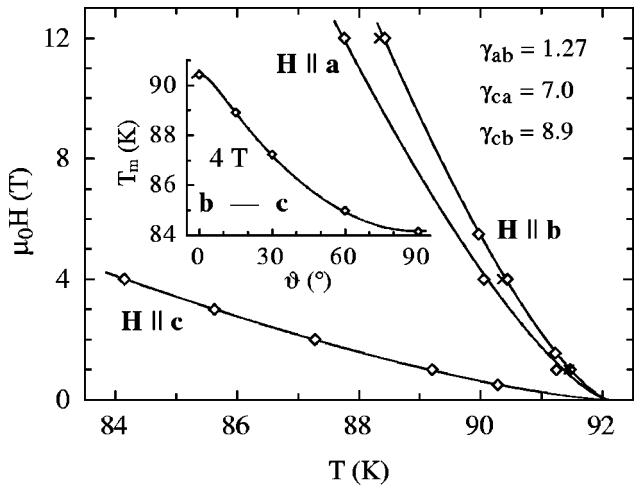


FIG. 4. Magnetic phase diagram around the melting transition for **H** directed along the *c* axis and 1° from the *a* and *b* axes. The curves are fitted to measured data points (symbols) using Eq. (1). For **H** ∥ **b** voltage measurements were made using two sets of potential contacts; $V_{15}$ ($\diamond$) and $V_{48}$ ($\times$). The inset shows the melting temperature as a function of magnetic-field direction at 4 T when the field is rotated from nearly **H** ∥ **b** ($\vartheta = 1°$) to **H** ∥ **c** ($\vartheta = 90°$). The curve is calculated using parameters obtained from the fitted curves in the main figure.

### B. Anisotropy from the vortex phase diagram

In Fig. 4 the experimentally determined melting transitions $H_m(T)$ are shown for **H** ∥ **c** and **H** aligned 1° away from **a** and **b** towards the *c* axis. Since $H_m$ is anisotropy dependent, the measurements in the figure present an independent method to determine both in- and out-of-plane anisotropies. The way anisotropy affects the melting transition is well known and understood,[24–27] even though there are some quantitative differences in the actual temperature dependence between theory and experiments. For the present case with anisotropy both within the plane and between the plane and the *c* axis, we used the relation

$$H_m = \frac{H_0}{\gamma_{ca}\gamma_{cb}\varepsilon_{\vartheta,\varphi}}\left(1-\frac{T}{T_c}\right)^n, \qquad (1)$$

where

$$\varepsilon_{\vartheta,\varphi} = \left(\sin^2\vartheta + \frac{\cos^2\vartheta\cos^2\varphi}{\gamma_{ca}^2} + \frac{\cos^2\vartheta\sin^2\varphi}{\gamma_{cb}^2}\right)^{1/2}. \qquad (2)$$

Here $H_0$ is a constant, $\gamma_{ca}$ and $\gamma_{cb}$ the out-of-plane anisotropies, $\vartheta$ the angle from the $ab$ plane to the *c* axis, and $\varphi$ the angle from the *a* axis to the *b* axis. The temperature dependence of Eq. (1) is known to give a good description of experiments on YBCO using an exponent *n* in the range 1.3–1.5 (Refs. 27–30). The angular dependence of Eq. (2) was obtained by extending the general anisotropic scaling approach by Blatter *et al.*[26] to include in-plane anisotropy.

By taking $T_c = 92.1$ K, $n = 1.4$ and adjusting $H_0$, $\gamma_{ca}$, and $\gamma_{cb}$, Eq. (1) was fitted to the measured data points, generating the three curves seen in the main part of Fig. 4. The anisotropies were found to be $\gamma_{ca} = 7.0$ and $\gamma_{cb} = 8.9$, resulting in an in-plane anisotropy $\gamma_{ab} = 1.27$. To further check the consistency of these values, we used the obtained parameters and Eqs. (1) and (2) to calculate $T_m(\vartheta)$ for $\mu_0 H = 4$ T (**H** in the $bc$ plane). Our measurements are well described by the calculated curve, as seen in the inset of Fig. 4. The in-plane anisotropy obtained from the zero-field resistivities has a value $\gamma_{ab} \approx 1.32$ at $T_c$, but displays a rather strong temperature dependence. By extrapolating this resistive anisotropy from just above $T_c$ to lower temperatures, we estimate $\gamma_{ab} = 1.23$ at 85 K. The anisotropy as determined from the vortex phase diagram is, thus, consistent also with the resistive anisotropy in zero field.

Various values of $\gamma_{ab}$ for YBCO can be found in the literature. From early Bitter pattern decorations Dolan *et al.*[31] obtained an in-plane anisotropy of 1.13, comparable to results from magnetic-torque measurements[29,30,32] and small-angle neutron scattering[33] ($\gamma_{ab} = 1.12$–$1.18$). Values reported from infrared spectroscopy measurements,[34] modulation of Josephson critical current,[35] and scanning tunneling microscopy[36] are usually larger (in the range 1.2–1.7) but also less certain. More detailed comparisons are rendered difficult by the fact that $\gamma_{ab}$ varies both with temperature and oxygen deficiency.

### C. Origin of vortex-liquid dissipation

Let us now further discuss the origin of dissipation in the mixed state. It is clear that dissipation in the vortex solid at high currents is caused by vortex motion under the action of the Lorentz force. The vortex lattice in YBCO is pinned at low current densities, but a system without pinning defects or above the depinning critical current would become dissipative. The solid should still be able to carry a supercurrent *along* the applied magnetic field, though, which the vortex liquid cannot do.[16,17] Surface barriers have been found to affect the resistive behavior of Bi-2212 around $T_m$.[37] We have not observed such signatures in the present case, which is also in agreement with the results of Ref. 21. The difference in field strength where melting steps occur for Bi-2212 and YBCO may explain why surface barrier effects appear to be significant only for Bi-2212.

When the magnetic field is aligned exactly within the plane, the macroscopic Lorentz force contribution to the vortex-liquid resistivity disappears, as illustrated in the main part of Fig. 5. Intrinsic pinning from the layered structure, thus, effectively inhibits the motion of vortices perpendicular to the layers, at least at low currents. If instead the *c*-axis resistivity is studied, not changing the condition **H** $\perp$ **c**, the sharp step at $T_m$ is found to be unaffected by the intrinsic pinning.[38–40] This indicates that the solid-to-liquid transition stays first order even when the field is aligned within the plane. In the **j** ∥ **c** case the driving force acts along the planes. Hence the vortices do not need to pass any pinning barriers to move.

The resistivity that remains when the macroscopic Lorentz force contribution has been suppressed by the intrinsic pinning is almost independent of the angle between current and magnetic field. This is illustrated in the inset of Fig. 5. The observation leads to the question whether the remaining

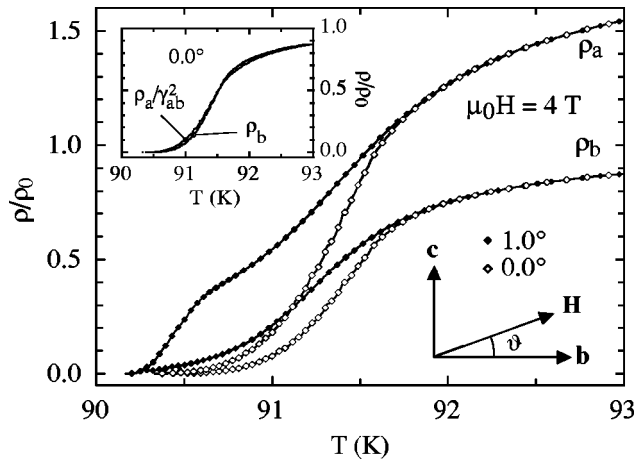


FIG. 5. Normalized resistivity as a function of temperature at 4 T for $\vartheta = 0.0°$ and 1.0°. For **H** aligned exactly within the plane all signs of the melting step disappear. Inset: At $\vartheta = 0.0°$ the *a*-axis resistivity (**j** $\perp$ **H**) normalized by the estimated $\gamma_{ab}^2(T)$ agrees fairly well with the *b*-axis resistivity (**j** $\parallel$ **H**).

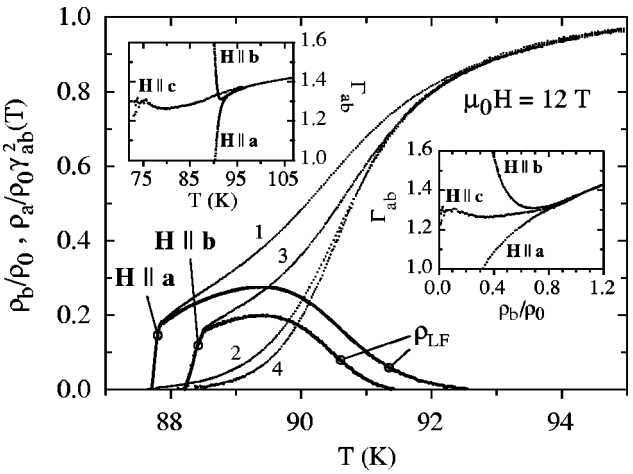


FIG. 6. Determination of the contribution from the macroscopic Lorentz force to the resistivity. The *a*-axis resistivities for the two field directions (curves 2 and 3) are normalized by $\gamma_{ab}^2(T)$. Thick curves correspond to the differences between the Lorentz force and force-free configurations, $\rho_{LF} = \rho_\perp - \rho_\parallel$, for the two field directions. Upper inset: In-plane resistive ratio at 12 T (0 T above 95 K) as a function of temperature and magnetic-field direction. Note the difference between $\Gamma_{ab}$ with **H** along the *c* axis and $\Gamma_{ab}$ with **H** in the plane at temperatures around $T_c$. Lower inset: If $\Gamma_{ab}$ is expressed as a function of resistivity level instead of temperature, the apparent discrepancy around $T_c$ vanishes. [Curves 1 and 2 (**H** $\parallel$ **a**) were obtained from measurements of $V_{67}$. Curves 3 and 4 (**H** $\parallel$ **b**) were based on measurements of $V_{48}$.]

resistivity should equal the longitudinal resistivity $\rho_\parallel$ for the case without intrinsic pinning. Our results do not fully answer this question. Comparing the two $\rho_b$ curves of the main figure, the longitudinal resistivity seems, at first glance, to have been further decreased by the pinning. More likely, however, the difference could arise from the small but finite *c*-axis component in the vortex direction, i.e., from the 1° misalignment.

The Lorentz force contribution to the resistivity can be determined by calculating $\rho_{LF} = \rho_\perp - \rho_\parallel$. When doing so, it is important to leave $T_m$ and other vortex properties unchanged. One, therefore, needs to keep the same field direction when determining $\rho_\perp$ and $\rho_\parallel$. This requires either different samples or the use of a pseudoflux transformer configuration. The resistivities finally have to be rescaled to a common level above $T_c$. Due to the rather strong temperature dependence of the resistive anisotropy, we assumed a simple, linear extrapolation of the zero-field resistive anisotropy as an estimate of $\gamma_{ab}(T)$. The rescaled $\rho_a$ curves then agree well with the unscaled $\rho_b$ data above $T_c$, as seen in Fig. 6. The resulting $\rho_{LF}$ curves are also shown in the main panel of the figure. We note that the **H** $\parallel$ **a** case seems to require a lower Lorentz force to yield the same corresponding vortex flow.

Although the difference in $T_m$ may partly make direct comparisons impossible, an analysis of the field dependence of $\rho_{LF}$ nevertheless reveals that the maximum $\rho_{LF}$ decreases for **H** $\parallel$ **b** with decreasing magnetic field, while it stays constant or increases slightly for **H** $\parallel$ **a** (not shown). At 1 T only a small fraction remains of $\rho_{LF}$ for **H** along the *b* axis, indicating a lower critical field around 1 T for this field direction. This is in qualitative agreement with the bottom panel of Fig. 2, where the upturn in $\Gamma_{ab}$ is almost absent at 1 T. The field $H_{lcp}$ at the lower critical point depends on correlated disorder or strong point defects.[41–43] Figure 1 indicates that $H_{lcp}$ in our sample is slightly below 0.5 T for **H** $\parallel$ **c**, which is in line with earlier observations.[41] Comparing this with the top and bottom panels of Fig. 2, we see that there is no direct connection between $H_{lcp}$ and $\varepsilon_{\vartheta,\varphi}$. This is astonishing, since the upper critical point $H_{ucp}$ is substantially increased for the in-plane directions. A plausible explanation could be that the lower critical point, unlike the upper critical point, is connected to a matching effect. It has been found that the state below $H_{lcp}$ is well described in terms of a Bose glass.[41] The difference in $H_{lcp}$ between the two in-plane directions may, thus, indicate a pinning effect from the copper-oxygen chains or from the oxygen vacancies within the chains.

Going back to the discussion of Fig. 6, we see that $\rho_{LF}$ extends to the vicinity of $T_c$. Unfortunately, a better knowledge of the temperature dependence of the extrapolated in-plane anisotropy is required to determine the exact location of zero Lorentz resistivity, i.e., where the direction of the applied magnetic field has no influence on the dissipation. It has been suggested that the vortex liquid should be divided into two well-defined regions, where only the low temperature part would have a nonzero vortex-line tension.[16] We would expect a dramatic drop of $\rho_{LF}$ to zero if the line tension would suddenly vanish. Instead, Fig. 6 indicates a gradual loss of line tension until $T_c$ is reached.

### D. Contribution from fluctuations

In the upper inset of Fig. 6 we show the in-plane resistive ratio $\Gamma_{ab} = (\rho_a/\rho_b)^{1/2}$ as a function of temperature. For **H** $\parallel$ **c** there is no reason why $\Gamma_{ab}$ should not equal $\gamma_{ab}$. Around $T_c$ the **H** $\parallel$ **a** and **H** $\parallel$ **b** curves for $\Gamma_{ab}$ come together and here again one could expect $\Gamma_{ab}$ to represent the true in-plane

anisotropy. Why then is the anisotropy lower in a small temperature range close to $T_c$ when the field lies within the plane? One possible explanation could be the influence of superconducting fluctuations. The fluctuation magnetoconductivity can be calculated directly from magnetoresistivity, $\Delta\sigma^{\mathrm{fl}}(H,T)=\sigma^{\mathrm{fl}}(H,T)-\sigma^{\mathrm{fl}}(0,T)\approx-\Delta\rho(H,T)/\rho^2(0,T)$ assuming a field independent normal-state resistivity. According to theory, the fluctuation anisotropy $\gamma_{ab}^{\mathrm{fl}}=(\sigma_b^{\mathrm{fl}}/\sigma_a^{\mathrm{fl}})^{1/2}=(\Delta\sigma_b^{\mathrm{fl}}/\Delta\sigma_a^{\mathrm{fl}})^{1/2}$ should be both field and temperature independent for $\mathbf{H}\parallel\mathbf{c}$ (Ref. 44). If the experimental conductivity is a sum of the normal state and fluctuation conductivities $\sigma=\sigma^N+\sigma^{\mathrm{fl}}$, the anisotropy $\gamma_{ab}$ will depend on the amount of fluctuations, following

$$\gamma_{ab}^2=(\gamma_{ab}^N)^2\frac{\rho_b^N+\rho_b^{\mathrm{fl}}}{(\gamma_{ab}^N/\gamma_{ab}^{\mathrm{fl}})^2\rho_b^N+\rho_b^{\mathrm{fl}}}. \tag{3}$$

Here $\gamma_{ab}^N=(\rho_a^N/\rho_b^N)^{1/2}$ and $\rho^N$ is the normal-state resistivity expected in the absence of fluctuations (usually extrapolated from high temperatures). The fluctuations are diminished by magnetic field, an effect that also depends on the orientation of the field. For $\mathbf{H}\parallel\mathbf{c}$ the upper critical field $H_{c2}$ is comparatively small. A 12 T field, therefore, can substantially reduce the amount of fluctuations, bringing the system closer to the normal state. With the same field applied along the $ab$ plane the change is less pronounced due to the larger in-plane $H_{c2}$. Calculating $a$- and $b$-axis resistivities from measurements shown in Fig. 1 ($\mathbf{H}\parallel\mathbf{c}$) at a temperature corresponding to the anomalous region in Fig. 6 and using the definition $\Delta\rho(H,T)=\rho(H,T)-\rho(0,T)$, we obtain $\gamma_{ab}^{\mathrm{fl}}\sim1.1$ in agreement with recent results from magnetoconductivity measurements.[45] This low-fluctuation anisotropy, thus, results in a higher $\gamma_{ab}$ when $\mathbf{H}\parallel\mathbf{c}$ than when the same field is applied along the $ab$ plane.

The anomaly around $T_c$ is resolved if $\Gamma_{ab}$ is plotted as a function of $\rho$ instead of $T$, as shown in the lower inset of Fig. 6. This observation agrees with Eq. (3) and indicates that vortex liquid properties are suitably studied at constant resistivity levels. Measurements on the vortex liquid close to the glass transition support this conclusion.[46]

## IV. SUMMARY AND CONCLUSIONS

We have presented modified flux transformer measurements where the vortex liquid was studied in different magnetic-field directions and Lorentz-force configurations. The results were interpreted with local conductivity, vortex-line motion, and a Lorentz-force-driven resistivity. A relatively large Lorentz force contribution was found by studying the resistivities parallel and perpendicular to the field. This contribution was suppressed when the field was exactly parallel to the $ab$ plane, as vortex motion was prohibited by the intrinsic pinning from $CuO_2$ planes. The resulting, featureless transition rather well agreed with the longitudinal resistivity, i.e., with the resistivity in the magnetic-field direction.

We further studied in-plane anisotropy effects on the vortex behavior and determined both in- and out-of-plane anisotropies from the field-temperature phase diagram. The in-plane anisotropy deduced from resistivity data was found to be higher than what fluctuation measurements suggest, indicating the presence of almost isotropic fluctuations. The varying amount of such fluctuations was suggested to cause the relatively strong temperature dependence of the resistive anisotropy around and below $T_c$.

## ACKNOWLEDGMENTS

Support from the Swedish Research Council for Engineering Sciences (TFR) and the Swedish Foundation for Strategic Research (SSF) under the OXIDE program is gratefully acknowledged.

*Electronic address: therese@ftf.kth.se

[1] R. Busch, G. Ries, H. Werthner, G. Kreiselmeyer, and G. Saemann-Ischenko, Phys. Rev. Lett. **69**, 522 (1992).
[2] H. Safar, E. Rodriguez, F. de la Cruz, P. L. Gammel, L. F. Schneemeyer, and D. J. Bishop, Phys. Rev. B **46**, 14 238 (1992).
[3] H. Safar, P. L. Gammel, D. A. Huse, S. N. Majumdar, L. F. Schneemeyer, D. J. Bishop, D. López, G. Nieva, and F. de la Cruz, Phys. Rev. Lett. **72**, 1272 (1994).
[4] Yu. Eltsev, W. Holm, and Ö. Rapp, Phys. Rev. B **49**, 12 333 (1994).
[5] D. López, G. Nieva, and F. de la Cruz, Phys. Rev. B **50**, R7219 (1994).
[6] E. Zeldov, D. Majer, M. Konczykowski, V. B. Geshkenbein, V. M. Vinokur, and H. Shtrikman, Nature (London) **375**, 373 (1995).
[7] A. Schilling, R. A. Fischer, N. E. Phillips, U. Welp, D. Dasgupta, W. K. Kwok, and G. W. Crabtree, Nature (London) **382**, 791 (1996).
[8] D. López, E. F. Righi, G. Nieva, and F. de la Cruz, Phys. Rev. Lett. **76**, 4034 (1996).
[9] G. Carneiro, Phys. Rev. Lett. **75**, 521 (1995).
[10] X. Hu, S. Miyashita, and M. Tachiki, Phys. Rev. Lett. **79**, 3498 (1997).
[11] A. K. Nguyen and A. Sudbø, Phys. Rev. B **58**, 2802 (1998).
[12] E. F. Righi, S. A. Grigera, G. Nieva, D. López, and F. de la Cruz, Phys. Rev. B **55**, 14 156 (1997).
[13] T. J. Hagenaars and E. H. Brandt, Phys. Rev. B **56**, R11 435 (1997).
[14] Y. Nonomura, X. Hu, and M. Tachiki, Phys. Rev. B **59**, R11 657 (1999).
[15] A. Rydh and Ö. Rapp, Phys. Rev. Lett. **86**, 1873 (2001).
[16] S-K. Chin, A. K. Nguyen, and A. Sudbø, Phys. Rev. B **59**, 14 017 (1999).
[17] A. K. Nguyen and A. Sudbø, Phys. Rev. B **60**, 15 307 (1999).
[18] W. K. Kwok, U. Welp, G. W. Crabtree, K. G. Vandervoort, R. Hulscher, and J. Z. Liu, Phys. Rev. Lett. **64**, 966 (1990).
[19] P. Olsson and S. Teitel, Phys. Rev. Lett. **82**, 2183 (1999).
[20] D. L. Kaiser, F. Holtzberg, M. F. Chisholm, and T. K. Worthington, J. Cryst. Growth **85**, 593 (1987).
[21] D. López, W. K. Kwok, H. Safar, R. J. Olsson, A. M. Petrean, L.

Paulius, and G. W. Crabtree, Phys. Rev. Lett. **82**, 1277 (1999).
[22] W. K. Kwok, U. Welp, V. M. Vinokur, S. Fleshler, J. Downey, and G. W. Crabtree, Phys. Rev. Lett. **67**, 390 (1991); W. K. Kwok, J. Fendrich, U. Welp, S. Fleshler, J. Downey, and G. W. Crabtree, *ibid.* **72**, 1088 (1994).
[23] D. López, E. F. Righi, G. Nieva, F. de la Cruz, W. K. Kwok, J. A. Fendrich, G. W. Crabtree, and L. Paulius, Phys. Rev. B **53**, R8895 (1996).
[24] A. Houghton, R. A. Pelcovits, and A. Sudbø, Phys. Rev. B **40**, 6763 (1989).
[25] Z. Hao and J. R. Clem, Phys. Rev. B **46**, R5853 (1992).
[26] G. Blatter, V. B. Geshkenbein, and A. I. Larkin, Phys. Rev. Lett. **68**, 875 (1992).
[27] W. K. Kwok, S. Fleshler, U. Welp, V. M. Vinokur, J. Downey, G. W. Crabtree, and M. M. Miller, Phys. Rev. Lett. **69**, 3370 (1992).
[28] A. Junod, M. Roulin, J.-Y. Genoud, B. Revaz, A. Erb, and E. Walker, Physica C **275**, 245 (1997).
[29] M. Willemin, A. Schilling, H. Keller, C. Rossel, J. Hofer, U. Welp, W. K. Kwok, R. J. Olsson, and G. W. Crabtree, Phys. Rev. Lett. **81**, 4236 (1998).
[30] T. Ishida, K. Okuda, A. I. Rykov, S. Tajima, and I. Terasaki, Phys. Rev. B **58**, 5222 (1998).
[31] G. J. Dolan, F. Holtzberg, C. Feild, and T. R. Dinger, Phys. Rev. Lett. **62**, 2184 (1989).
[32] T. Ishida, K. Inoue, K. Okuda, H. Asaoka, Y. Kazumata, K. Noda, and H. Takei, Physica C **263**, 260 (1996); T. Ishida, K. Okuda, H. Asaoka, Y. Kazumata, K. Noda, and H. Takei, Phys. Rev. B **56**, 11 897 (1997); T. Ishida, K. Okuda, and H. Asaoka, J. Low Temp. Phys. **117**, 1387 (1999).
[33] S. T. Johnson, E. M. Forgan, S. H. Lloyd, C. M. Aegerter, S. L. Lee, R. Cubitt, P. G. Kealey, C. Ager, S. Tajima, A. Rykov, and D. McK. Paul, Phys. Rev. Lett. **82**, 2792 (1999).
[34] D. N. Basov, R. Liang, D. A. Bonn, W. N. Hardy, B. Dabrowski, M. Quijada, D. B. Tanner, J. P. Rice, D. M. Ginsberg, and T. Timusk, Phys. Rev. Lett. **74**, 598 (1995).
[35] A. G. Sun, S. H. Han, A. S. Katz, D. A. Gajewski, M. B. Maple, and R. C. Dynes, Phys. Rev. B **52**, R15 731 (1995).
[36] I. Maggio-Aprile, Ch. Renner, A. Erb, E. Walker, and Ø. Fischer, Phys. Rev. Lett. **75**, 2754 (1995).
[37] D. T. Fuchs, E. Zeldov, M. Rappaport, T. Tamegai, S. Ooi, and H. Shtrikman, Nature (London) **391**, 373 (1998).
[38] M. Charalambous, J. Chaussy, and P. Lejay, Phys. Rev. B **45**, 5091 (1992).
[39] N. E. Hussey, H. Takagi, N. Takeshita, N. Mori, Y. Iye, S. Adachi, and K. Tanabe, Phys. Rev. B **59**, R11 668 (1999).
[40] Yu. Eltsev and Ö. Rapp, Phys. Rev. B **60**, 14 621 (1999).
[41] W. K. Kwok, R. J. Olsson, G. Karapetrov, L. M. Paulius, W. G. Moulton, D. J. Hofman, and G. W. Crabtree, Phys. Rev. Lett. **84**, 3706 (2000).
[42] L. M. Paulius, W. K. Kwok, R. J. Olsson, A. M. Petrean, V. Tobos, J. A. Fendrich, G. W. Crabtree, C. A. Burns, and S. Ferguson, Phys. Rev. B **61**, R11 910 (2000).
[43] A. Schilling, R. A. Fisher, N. E. Phillips, U. Welp, W. K. Kwok, and G. W. Crabtree, Phys. Rev. Lett. **78**, 4833 (1997).
[44] K. Maki and R. S. Thompson, Phys. Rev. B **39**, 2767 (1989).
[45] T. Björnängen, J. Axnäs, Yu. Eltsev, A. Rydh, and Ö. Rapp, Phys. Rev. B **63**, 224518 (2001).
[46] A. Rydh, Ö. Rapp, and M. Andersson, Phys. Rev. Lett. **83**, 1850 (1999).